JACS
JOURNAL OF THE AMERICAN CHEMICAL SOCIETY
Article
pubs.acs.org/JACS

Efficient Long-Range Stereochemical Communication and Cooperative Effects in Self-Assembled Fe_4L_6 Cages

Naoki Ousaka,[†] Sergio Grunder,[‡] Ana M. Castilla,[†] Adam C. Whalley,[‡] J. Fraser Stoddart,*[,‡,§] and Jonathan R. Nitschke*[,†]

[†]Department of Chemistry, University of Cambridge, Lensfield Road, Cambridge CB2 1EW, United Kingdom

[‡]Department of Chemistry, Northwestern University, 2145 Sheridan Road, Evanston, Illinois 60208, United States

[§]NanoCentury KAIST Institute and Graduate School of EEWS (WCU), Korea Advanced Institute of Science and Technology (KAIST), 373-1 Guseong Dong, Yuseong Gu Daejeon 305-701, Republic of Korea

Supporting Information

ABSTRACT: A series of large, optically active Fe_4L_6 cages was prepared from linear 5,5′-bis(2-formylpyridines) incorporating varying numbers (n = 0−3) of oligo-*p*-xylene spacers, chiral amines, and Fe^{II}. When a cage was constructed from the ligand bridged by one *p*-xylene spacer (n = 1) and a bulky chiral amine, both a homochiral Fe_2L_3 helicate and Fe_4L_6 cage were observed to coexist in solution due to a delicate balance between steric factors. In contrast, when a less bulky chiral amine was used, only the Fe_4L_6 cage was observed. In the case of larger cages (n = 2, 3), long-range (>2 nm) stereochemical coupling between metal centers was observed, which was minimally diminished as the ligands were lengthened. This communication was mediated by the ligands' geometries and rigidity, as opposed to gearing effects between xylene methyl groups: the metal-centered stereochemistry was not observed to affect the axial stereochemistry of the ligands.

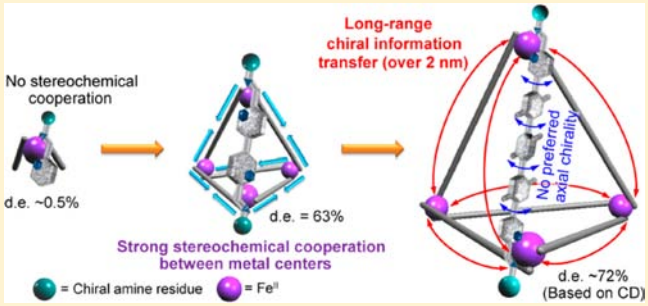

INTRODUCTION

Self-assembled metal−organic cages[1−7] with specified stereochemistry can provide chirotopic inner phases for stereoselective guest encapsulation and sensing[8−13] as well as asymmetric reactions.[14−18] The construction of larger, well-defined chiral inner spaces presents a challenge because an increase in ligand length leads to an increase in cage flexibility, allowing a cage framework to more readily adopt multiple stereochemical configurations. The degree of stereochemical definition of a cage's inner phase is thus eroded, reducing its usefulness in the applications noted above. Fundamental studies are thus necessary into the transmission of stereochemical information within larger cage frameworks, in order to determine whether larger guests, with a higher degree of chemical functionalization, might be bound and transformed within a given class of cages.

The technique of subcomponent self-assembly has recently enabled the construction of a variety of tetrahedral M_4L_6 cages.[19−22] These cages, assembled from six-coordinate iron(II) ions and C_2-symmetric bis(bidentate) ligands based on benzidine[19,20] and bipyridine[21,22] derivatives via the *in situ* formation of dynamic-covalent imine bonds,[23−25] have been observed to form racemic mixtures of homochiral structures with approximate T-symmetry,[19−21,26−32] in which all four metal centers have the same metal-centered configuration (ΔΔΔΔ/ΛΛΛΛ). When chiral-amine subcomponents were incorporated into the vertices of bipyridine-based cages, strong cooperative stereochemical coupling between metal centers was observed.[22]

However, when *p*-diamino-terphenyl derivatives and 2-formylpyridine were used as cage subcomponents,[33] the resulting Fe_4L_6 cages were observed to form mixtures of homochiral T (ΔΔΔΔ/ΛΛΛΛ), heterochiral C_3 (ΔΔΔΛ/ΛΛΛΔ), and achiral S_4 (ΔΔΛΛ) diastereomers.[33−37]

Cooperative interactions between asymmetric centers have been observed to lead to nonlinear enhancements in chiroptical properties, which have been studied in helical polymers[38−44] and other (macro-) supramolecular systems.[45−48] In these cases, the helical sense bias is amplified in the presence of small proportions of chiral units in the helically folded achiral main chain.[38−48] Additionally, rigid helical structures (in which there is a high energetic penalty of helical reversal) enable long-range stereochemical communication and end-to-end chiral information transmission along a helical chain composed of achiral units.[49−53] However, to our knowledge, these examples of chiral information transfer have been limited to helical molecules so far because unstable helical structures or helical molecules containing a helix-disturbing segment lose their stereochemical information completely during the relay step.[54−56]

Received: July 6, 2012
Published: August 23, 2012

   dx.doi.org/10.1021/ja306615d | J. Am. Chem. Soc. 2012, 134, 15528−15537

Herein we report an example of long-range (>2 nm) stereochemical communication and cooperativity within tetrahedral Fe_4L_6 cages. The ligands of these cages were observed to effectively mediate stereochemical communication between Fe^{II} stereocenters, despite these ligands' adoption of a nonhelical structure. As shown in Scheme 1, our chosen ligands

Scheme 1. Diastereoselective Formation of Tetrahedral Fe_4L_6 Cages 1a−4a (with Less Bulky Chiral Amine A) and 1b−4b (with Bulky Chiral Amine B)[a]

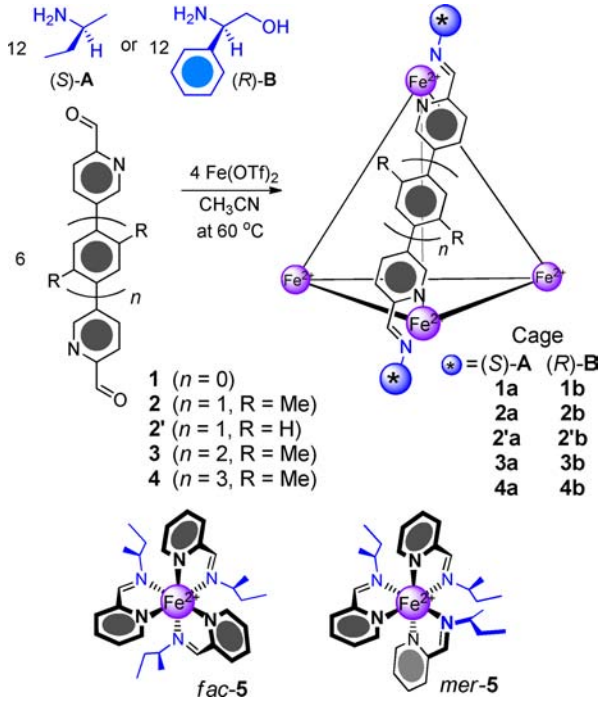

[a]Only one ligand is drawn for clarity. Mononuclear complexes *fac*- and *mer*-**5** are also shown.

consist of 5,5′-bis(2-formylpyridines) bridged by varying numbers of oligo-*p*-xylene spacers (n = 0−3)[57−60] as subcomponents. The moderate barrier to bond rotation between the xylene rings leads to slow interconversion between *P* and *M* axial conformations of the ligands on the NMR time scale,[59,60] which allowed us to infer details as to the axial conformations of the xylene ligand moieties in the cages. When the dialdehyde bridged by one *p*-xylene spacer and bulky chiral amine **B** shown in Scheme 1, which has been observed to quantitatively induce a single stereochemical configuration at the Fe^{II} centers,[61−64] were used as the subcomponents, a Fe_2L_3 helicate and Fe_4L_6 cage were observed to coexist in equilibrium. In contrast, only the Fe_4L_6 cage is observed when less-bulky chiral amine **A** shown in Scheme 1, which only moderately biases the Fe^{II}-centered configuration, was used. This sterically induced formation of the helicate structure was not observed in other cases. Even though the metal-centered configuration did not affect the ligand's axial chirality (no gearing effect[49−53] was observed) in cages with the longer ligands, efficient long-range stereochemical interaction between metal centers was observed to take place.

RESULTS AND DISCUSSION

Subcomponents **2**−**4** were synthesized from the corresponding boronic ester derivatives and 5-bromo-2-formylpyridine by Pd-catalyzed Suzuki−Miyaura cross-coupling.[65,66] A full description of syntheses is provided in the Supporting Information.

We chose the amines (*S*)-2-aminobutane [(*S*)-**A**] and (*R*)-phenylglycinol [(*R*)-**B**] as chiral subcomponents for this study. The latter is known to quantitatively induce a single stereochemical configuration at the metal center in the mononuclear Fe^{II} tris(pyridylimine) complex, through steric and π-stacking effects between phenyl and pyridyl rings.[61−64] In contrast, the former is a less bulky amine, which was expected to have a weaker influence on the stereochemistry of the metal center.

The reaction between dialdehyde **1**−**4** (6 equiv), chiral amine **A** or **B** (12 equiv), and iron(II) trifluoromethanesulfonate [$Fe(OTf)_2$] (4 equiv) in acetonitrile produced cages **1a**−**4a** [from (*S*)-**A**] and **1b**−**4b** [from (*R*)-**B**], as shown in Scheme 1. All cages were characterized by ^1H, ^{13}C, and diffusion ordered spectroscopy (DOSY, except for **2′a** and **2′b**) NMR, electrospray ionization mass spectroscopy (ESI-MS, Figures S1 and S2), and circular dichroism (CD) measurements. The diffusion coefficients (D) of each cage, obtained from diffusion-ordered NMR spectroscopy (DOSY) measurements, were consistent with the existence of only one species in solution, except for **2b** (*vide infra*) (Figures S3 and S4). A linear correlation was observed between the number of *p*-xylene spacers in the ligand and the D value determined for the corresponding cage (Figure 1B), in keeping with the linear increase in cage size predicted by molecular modeling (MM+ force field, Figure 1A).[67]

Short-Range Stereochemical Communication. In order to estimate the degree of stereochemical coupling between the Fe^{II} centers in cage **1a**, the diastereomeric excess (de) values of **1a** and the analogous mononuclear complex **5** (Scheme 1), for which no cooperation is possible, were determined by ^1H NMR and confirmed by CD.

The ^1H NMR spectrum of **5** is complicated due to the presence of *fac*-Δ, *fac*-Λ, *mer*-Δ, and *mer*-Λ diastereomers, resulting in the presence of eight sets of signals, although only six sets of imine peaks were observed due to partial overlapping (Figure S5). Deconvolution of the imine peak clusters,[68] however, allowed the determination of de values (Table 1) (*fac*/*mer* = 45/55). Therefore, the less bulky chiral amine (*S*)-**A** did not induce a strong stereochemical preference at the Fe^{II} center.

The ^1H NMR spectrum of **1a** at 293 K (Figure 2A) showed four distinct sets of signals. This spectrum was assigned to the ΔΔΔΔ and ΛΛΛΛ diastereomers, either empty or encapsulating one OTf^- anion per cage, with the cage geometry requiring all metal ions to adopt *fac* stereochemistry.[22] At 343 K, only the empty cages were observed, with well-separated peaks, which could be integrated to estimate of the de value (63%). We attribute the increase in magnitude of this de over that of *fac*-**5** (∼0.5%) to strong cooperative stereochemical communication between the four Fe^{II} centers, such that the effects of individual chiral amine residues upon the stereochemistry of Fe^{II} centers is enhanced.

The pyridyl protons of **1b** showed upfield shifts as compared to those of **1a** due to shielding effects from the stacked phenyl rings ($\Delta\delta$ = 0.41−0.76 ppm). In keeping with prior results,[22] the ^1H NMR spectrum of **1b** at 298 K shows two distinct sets of signals, corresponding to the empty cage and the cage encapsulating one OTf^- anion (Figure S6).

The ratio between empty and full **1b** was again sensitive to changes in temperature, with guest anion release being

dx.doi.org/10.1021/ja306615d | J. Am. Chem. Soc. 2012, 134, 15528−15537

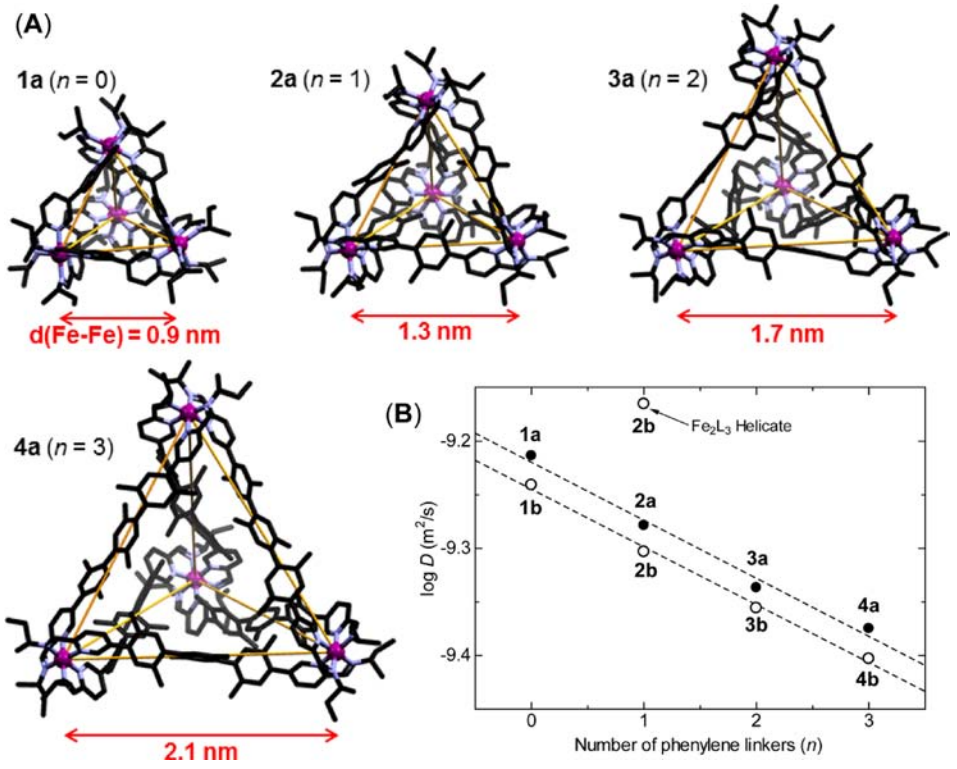

Figure 1. (A) Molecular models of cages **1a**–**4a** (ΔΔΔΔ-diasteromers) optimized by molecular mechanics (MM+ force field). Only one of the possible diasteromers with respect to axial chirality (*P* or *M*) of the ligands is shown. Hydrogen atoms are omitted for clarity. (B) Plots of diffusion coefficients (log *D*) vs number of phenylene linkers of cage's ligand. All DOSY spectra were measured under the same conditions (298 K, [Fe^{II}] = 4.0 mM). The solid circles correspond to **1a**–**4a** and the open circles to **1b**–**4b**, respectively. DOSY spectra are shown in Figures S3 and S4.

Table 1. Diastereomeric Excess (de) Values of 1a–4a and 5

compound	de (%)
fac-**5**	ca. 0.5[a]
mer-**5**	ca. 16[a]
1a	63[a]
2a	89[a]
2′a	79[a]
3a	74[b]
4a	72[b]

[a]de determined by ^{1}H NMR integration. [b]de estimated by CD measurement.

observed at higher temperatures,[22] a phenomenon of possible interest in the context of stimulus-driven guest delivery. Filled cage **1b** was the only entity observed at 263 K, indicating the presence of only one diastereomer, in keeping with the observation that the analogous mononuclear Fe^{II} complex formed diastereoselectively.[62]

The CD intensity at the ligand-to-metal charge transfer (LMCT) band of **1a**, at ca. 300 nm, is larger than that of **1b**, despite the de of **1a** being smaller than that of **1b**. We attribute the more intense Cotton effects in the case of **1a** to interligand exciton coupling,[69,70] where CD and absorption spectral patterns in this region are different from each other. In particular, the absorption coefficient of **1b** around 300 nm is smaller than that of **1a** due to $\pi-\pi$ stacking between phenyl and pyridyl rings which usually leads to a hypochromic effect.[71–73] In contrast, the CD patterns of **1a** and **1b** are similar to each other, with different CD intensities, at the metal-

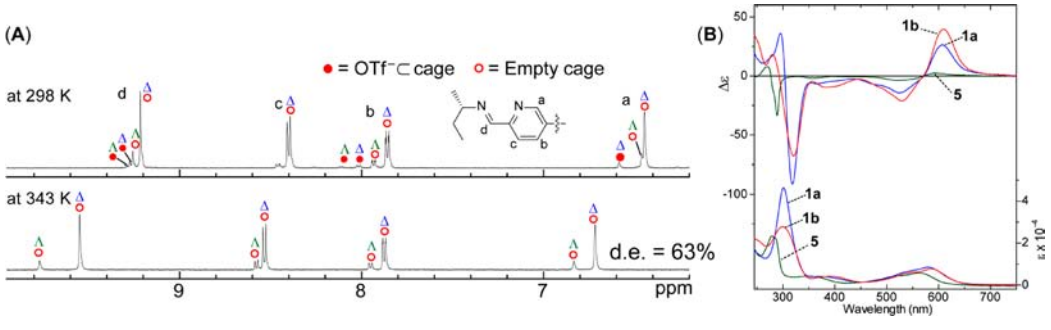

Figure 2. (A) ^{1}H NMR (500 MHz) spectra of cage **1a** in CD_3CN at 298 and 343 K; [**1a**] = 1.0 mM. The red solid and empty circles denote $OTf^- \subset$ **1a** and empty cage **1a**, respectively. (B) CD (top) and absorption (bottom) spectra of cages **1a** (blue lines), **1b** (red lines), and mononuclear complex **5** in CD_3CN/CH_3CN (1/5) mixture; [Fe^{II}] = 3.6–3.7 × 10^{-4} M. Δε and ε were normalized with respect to [Fe^{II}]. All spectra except for **5** were measured after heating at 60 °C for 2 days and then allowing to stand at room temperature for 1 day.

dx.doi.org/10.1021/ja306615d | *J. Am. Chem. Soc.* 2012, 134, 15528–15537

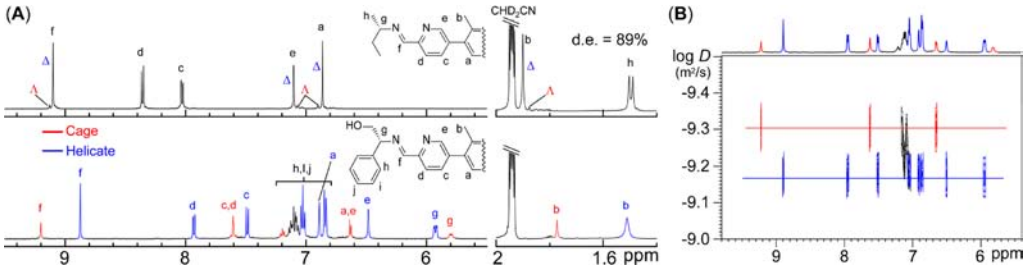

Figure 3. (A) ^{1}H NMR (500 MHz) spectra of cage **2a** (upper) and **2b** (bottom) in CD_3CN at 298 K; [Fe^{II}] = 4.0 mM. [helicate]:[cage] = 4:1. (B) DOSY spectrum of **2b** in CD_3CN at 298 K.

to-ligand charge transfer (MLCT) band above 450 nm (Figure 2B), consistent with a predominance of the ΔΔΔΔ-isomer.[22,61−64,74] The CD intensity at the first Cotton effect (609 nm) of **1a** ($\Delta\varepsilon^{first}$) is 1.5 times smaller than that of **1b**, which is in good agreement with the expected de values (de_{exp}) of **1a** that can be expressed by eq 1 below:

$$de_{exp} = \Delta\varepsilon^{first}/\Delta\varepsilon^{first}_{max} \times 100 \quad (1)$$

where $\Delta\varepsilon^{first}$ and $\Delta\varepsilon^{first}_{max}$ are the CD intensity of the mixture of diastereomeric cages and the maximum CD intensity of a diastereopure cage (de = 100%), respectively. Therefore, the CD intensity of **1a**, at 609 nm, is comparable with that of **1b**.[22,64] As expected by the lower de of complex **5** observed by ^{1}H NMR, its CD intensity was weak, deriving mainly from the *mer*-isomer (Δ-rich).

Mid-Range Stereochemical Communication. To clarify the effect of ligand extension on mid-range communication between Fe^{II} stereocenters, cages **2a** and **2b**, and their analogues **2′a** and **2′b** were prepared for comparison with cages **1a** and **1b**. The ^{1}H NMR spectrum of **2a** shows two distinct sets of signals assigned to the ΔΔΔΔ and ΛΛΛΛ diastereomers (Figure 3A). There is no observation of distinct peaks corresponding to the cage encapsulating a OTf^- anion and the empty cage, as observed in **1a** and **1b**. This is probably due to the fast exchange between these two species on the NMR time scale because of the cage's porous nature[75] or the weakness of its triflate binding. Interestingly, the de of **2a** (89%) is higher than that of **1a** despite the longer distance between Fe^{II} centers. Similarly, the de of analogous cage **2′a**, without methyl groups on the central phenyl ring, is 79% (Figures S7 and S8). These de values did not change after heating to 60 °C for 2 days. In order of increasing de, the series is thus: **1a** < **2′a** < **2a**. We attribute this ordering to the following three factors: (1) Molecular modeling (Figure 1A) and related crystal structures[21,22] suggest that in the case of cage **1a**, the bipyridine ligand is slightly bent toward the inner space of the cage, which leads to decreasing van der Waals interactions between pyridyl rings and the aliphatic groups derived from aminobutane; (2) in the case of cage **2′a**, this ligand bending is relaxed by the extension of one phenylene spacer, which may lead to an increase in van der Waals interaction at the corners; and (3) in the case of cage **2a**, the higher de value is probably due to steric interactions between methyl groups on the central phenylene spacer and aliphatic groups of the chiral amine residues, which are not present in the case of cage **2′a**.

Surprisingly, the ^{1}H NMR spectrum of **2b** showed two distinct sets of peaks with different diffusion coefficients, as measured by DOSY NMR (Figure 3). The ratio of hydrodynamic radii (r_s) between the species giving rise to these two sets of peaks is 1.37, consistent with the coexistence of a Fe_4L_6 cage (minor peaks, red line) and Fe_2L_3 triple helicate (major peaks, blue line) in a 1:4 ratio (Figures 1B and 3B). ESI-MS measurements are also consistent with the presence of both cage and helicate (Figure S2).

Raymond and co-workers have reported that a M_2L_3 triple helicate could be transformed into a M_4L_6 cage by the addition of a suitable guest.[76] However, our preliminary experiments revealed that the ratio between cage and helicate did not change by 10-fold dilution or by the addition of large excess of $Bu_4N^+TfO^-$ (103 equiv) as a prospective guest. In contrast, only the formation of Fe_4L_6 cage **2′b** (Figure S7) was observed from ligand **2′**, which bears no methyl groups on its central phenyl ring.

Molecular modeling studies of helicate **2b** and cages **2a** and **2b** suggested that steric crowding around the methyl groups on the central *p*-xylene and π-stacked phenyl rings in cage **2b** (Figure 4A), absent in cage **2a** (Figure 4B), are the main

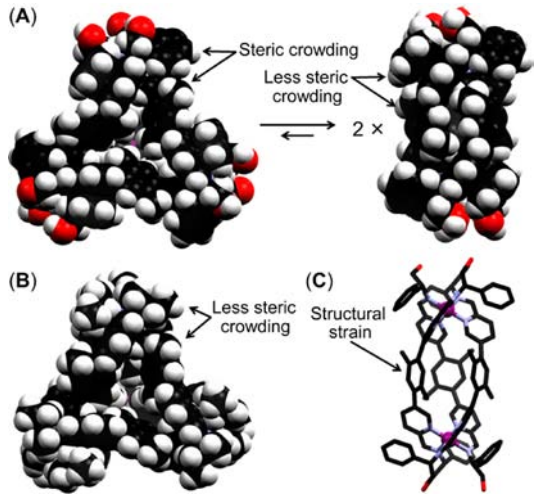

Figure 4. CPK models of cage/helicate (A) **2b** and (B) **2a** optimized by molecular mechanics calculations (MM+ force field). (C) Ball and stick representation of helicate **2b**.

driving forces for the formation of the helicate structure. This steric crowding is reduced in the helicate due to the bending of the ligand,[77,78] which in turn increases the structural strain (Figure 4A,C). We attribute the coexistence of cage and helicate structures in the singular case of **2b** to the competing energetic penalties between steric crowding and structural strain.

CD and absorption spectra of **2a** and **2b** at their LMCT bands are quite different because of the dominant contribution from the helicate component of **2b** (Figure 5A), whose ligand

dx.doi.org/10.1021/ja306615d | J. Am. Chem. Soc. 2012, 134, 15528−15537

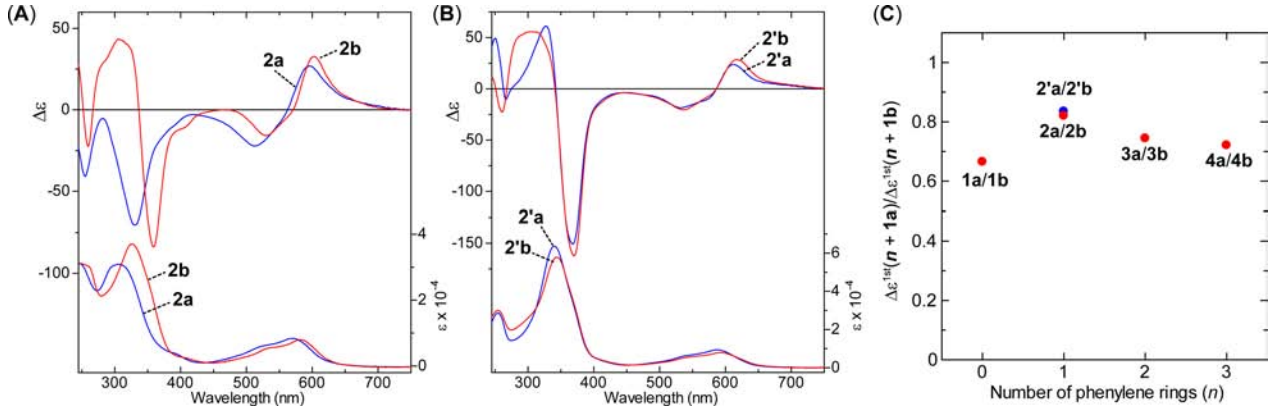

Figure 5. CD (top) and absorption (bottom) spectra of (A) **2a** (blue lines), **2b** (red lines) and (B) **2′a** (blue lines), **2′b** (red lines) in CD_3CN/CH_3CN (1/5) mixture; $[Fe^{II}] = 3.6 - 3.7 \times 10^{-4}$ M. $\Delta\varepsilon$ and ε were normalized with respect to $[Fe^{II}]$. All spectra were measured after heating at 60 °C for 48 h and then allowing to stand at room temperature for 24 h. (C) Plots of the relative CD intensities at first cotton effect around 600 nm between $(n + 1)$a and $(n + 1)$b vs number of phenylene rings (n).

conformation is different from that of the cage. As seen in the energy-minimized molecular models of cages **2a** and **2b** (Figure 4), one of the two methyl groups on each central phenylene ring is directed toward the inside of the cage, while the other is on the opposite side, resulting in each ligand adopting a *P*/*M* axial conformation (Chart 1). In contrast, the ligands of helicate **2b** adopt an *M*/*M* axial conformation. We attribute the red-shift in the LMCT absorption maximum of helicate **2b** (at 325 nm) relative to that of **2a** (at 305 nm) to an increase in π-conjugation reflected in a greater degree of coplanarity for the pyridyl and phenylene rings in the case of **2b**, as reflected in the greater average xylene−pyridine dihedral angles in **2a** than in **2b**. In contrast, the CD and absorption spectral patterns between the analogous cages **2′a** and **2′b** are very similar to each other (Figure 5B). As discused above, the $\Delta\varepsilon^{first}$ values of **2a** and **2′a** around 600 nm are comparable to those of **2b** and of **2′b**, respectively. Indeed, the relative CD intensities $\Delta\varepsilon^{first}(\mathbf{2a})/\Delta\varepsilon^{first}(\mathbf{2b})$ and $\Delta\varepsilon^{first}(\mathbf{2'a})/\Delta\varepsilon^{first}(\mathbf{2'b})$ are 0.82 and 0.83, respectively, which match reasonably well with each observed de value (Figure 5C). Therefore, the relative CD intensity can be used to estimate the de value not only for the smaller cages but also the larger cages if the $\Delta\varepsilon$ value at 100% de is known.

Chart 1. Schematic Representations of Ligand Conformations in Cages 2a and 2b and in Helicate 2b

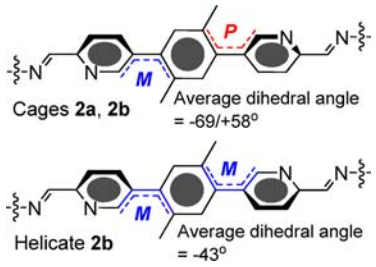

Long-Range Stereochemical Communication. The series of larger cages **3a**, **3b**, **4a**, and **4b** is composed of ligands in which the terminal pyridine rings are spaced apart by two or three *p*-xylene rings. The rate of axial isomerization between these rings was observed to be slow on the NMR time scale at room temperature,[60] whereas these rings were observed to rotate rapidly past the terminal pyridyl rings on the same time scale. Therefore, two axial conformations should be distinguishable for each ligand in **3a** and **3b** and three such configurations for **4a** and **4b** by NMR (Scheme 2).

Scheme 2. Interconversion between the Possible Conformations of the Ligand in Cages 3a and 3b and in Cages 4a and 4b

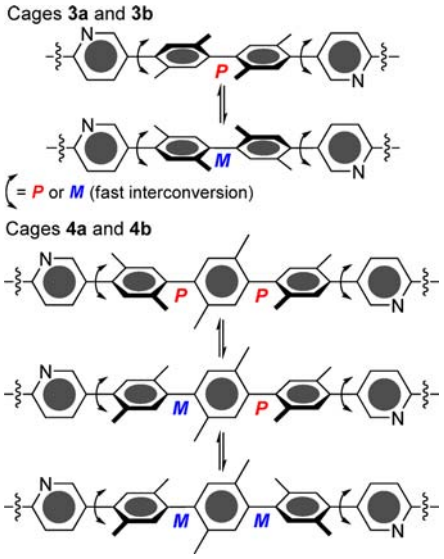

Relatively simple ^{1}H NMR spectra of these four cages were observed at 298 K, except for the phenylene and methyl resonances (Figures 6 and S9−S11). The pyridyl protons of **3b** and **4b** show upfield shifts compared to those of **3a** and of **4a**, respectively, indicating that the π-stacking mode observed in **1b** is also present in these larger cages. Unfortunately, de values of **3a** and **4a** could not be determined by NMR because of similar chemical shifts between ΔΔΔΔ and ΛΛΛΛ diastereomers, due probably to the lengthy distances between the Fe^{II} vertices of these structures (Figures S9 and S10).

Interestingly, **3b** and **4b** were observed to form only cages, in contrast with **2b** adopting both cage and helicate structures. The extension of the xylene chain is expected to lead to an increase in the number of possible orientations of the xylene ring adjacent to the pyridyl ring as a result of decreased steric crowding in comparison to **2b**. Six axial conformations are thus

dx.doi.org/10.1021/ja306615d | J. Am. Chem. Soc. 2012, 134, 15528−15537

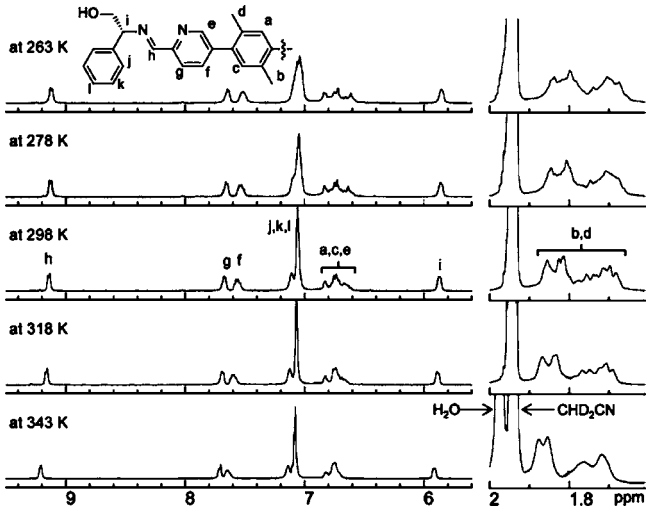

Figure 6. Variable-temperature ^{1}H NMR (500 MHz) spectra of cage **3b** in CD_3CN; [**3b**] = 1.0 mM.

possible for each ligand of **3b** (Figure 7). To avoid steric clash between the phenyl ring of the amine residue and the methyl

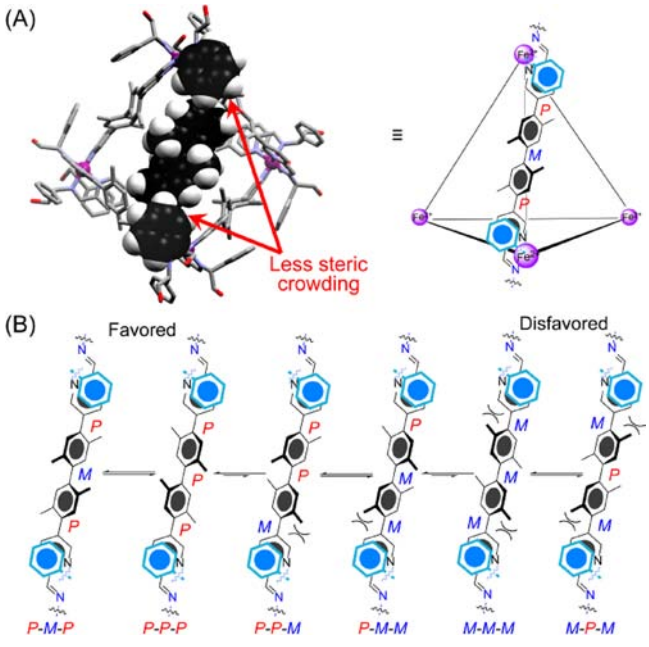

Figure 7. (A) Optimized (MM+ force field) molecular model of ΔΔΔΔ-**3b**. One of the possible diastereomers with respect to axial chirality (*P* and *M*) of the ligand is shown. The stacked phenyl rings of the chiral amine residues and the *p*-xylene rings are highlighted as a space-filling model. A schematic representation of the cage is also shown. The blue phenyl rings denote the stacked phenyl rings from the terminal amine residues. (B) The possible axially chiral conformations of the ligand in **3b**.

group closest to the pyridyl ring, the methyl group is predicted to preferentially orient into the center of the cage, leading to the preferential formation of *P*−*M*−*P* and *P*−*P*−*P* axial conformations for each ligand (*P*−*P*−*P*−*P*, *P*−*P*−*M*−*P*, and *P*−*M*−*M*−*P* for **4b**) (Figure 7B). In contrast, the absence of such steric interactions in cages **3a** and **4a** may lead to the prevalence of a larger number of ligand axial configurations.

There are many possible diastereomers of **3a** and **3b**, such as ΔΔΔΔ-(*PPPPPP*), (*PPPPPM*), (*PPPPMM*), (*PPPMMM*) and so on. If the cage forms only one diastereomer or the rate of axial isomerization is fast on the NMR time scale, this would result in the observation of only one set of signals, comprising two methyl proton signals from the xylene rings in **3a** and **3b** (three signals for **4a** and **4b**) due to the pseudo C_2-symmetry of the ligand. However, as shown in Figure 6, a large number of phenylene (a,c) and methyl proton (b,d) peaks were observed although each Fe^{II} center is expected to have Δ-stereochemistry, judging from the formation of only a single diastereomer in the analogous mononuclear complex.[62]

These peaks, which we attribute to different axially chiral conformations, grew more numerous at lower temperatures and partially coalesced at 343 K where four clusters of the methyl peaks were observed to remain. The 1:1:1:1 ratio of these clusters may correspond to *P* and *M* axially chiral conformations where the magnetic environments of each ligand are averaged. A similar behavior was also observed in cages **3a**, **4a**, and **4b** (the methyl proton signals of **4a** and **4b** were observed to overlap with the CHD_2CN residual solvent peak), indicating that the Fe^{II}-centered configuration does not affect the ligand's axial configurations, i.e., no gearing effect was observed.

CD and UV−vis absorption spectral patterns among **3a**, **3b**, **4a**, and **4b** above 300 nm are similar to each other (Figure 8). The relative CD intensities $\Delta\varepsilon^{first}$(**3a**)/$\Delta\varepsilon^{first}$(**3b**) and $\Delta\varepsilon^{first}$(**4a**)/$\Delta\varepsilon^{first}$(**4b**) are calculated to be 0.74 and 0.72, respectively, which are of comparable value to those of smaller cages (Figure 5C), indicating that long-range cooperative stereochemical communication between four Fe^{II} centers takes place with almost no loss of information even over 2 nm.

This unexpected long-range communication may be attributed to thermodynamic favoring of the *T*-symmetric cage framework, which was surprising because the Fe_4L_6 cage constructed from *p*-terphenylenediamine and 2-formylpyridine adopts *T*-, C_3-, and S_4-symmetries in nearly equal amounts;[33] an increase in the amounts of C_3- and S_4-symmetric cages implies a decrease in the degree of cooperative stereochemical communication between metal centers. To clarify why the *T*-symmetric framework appeared to be favored in the present system, we carried out molecular modeling studies on a S_4-symmetic cage, composed of ligand **3** without methyl groups, for simplicity, and *iso*-propylamine residues (cage S_4-**6**), alongside the previously reported *p*-terphenylenediamine-based cage (cage S_4-**7**).[33] As shown in Figure 9, the Fe^{II} ions in S_4-symmetric cages are connected by four *syn*-ligands (green) and two *anti*-ligands (black).[33−35,37] In the case of S_4-**7**, the ideal N···N distance between the opposite sides of the *syn*-ligand is virtually identical to that of *anti*-ligand because of the ligand geometry, wherein four nitrogen atoms are aligned (Figure 9B).[34,35] In contrast, the two N···N distances in S_4-**6** are different to each other because of the offset ligand geometry (Figure 9A), leading to distortions in the cage structure and a higher energetic penalty. This line of argument applies as well to C_3-symmetric cages, which have equal numbers of *syn*- and *anti*-ligands.[33−35] We infer, thus, that the degree of offset in such rigid ligand systems determines the degree of stereochemical communication between metal centers, as opposed to gearing effects between spacer groups.

dx.doi.org/10.1021/ja306615d | J. Am. Chem. Soc. 2012, 134, 15528−15537

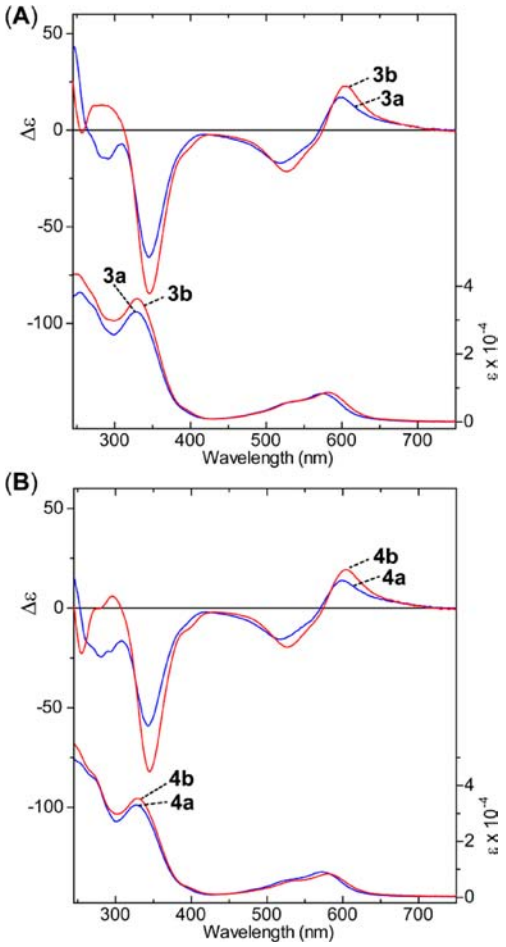

Figure 8. CD (top) and absorption (bottom) spectra of (A) **3a** (blue lines), **3b** (red lines), and (B) **4a** (blue lines), **4b** (red lines) in CD_3CN/CH_3CN (1/5) mixture; $[Fe^{II}] = 3.6–3.7 \times 10^{-4}$ M. $\Delta\varepsilon$ and ε were normalized with respect to $[Fe^{II}]$. All spectra were measured after equilibration at 60 °C for 48 h and then allowing to stand at room temperature for 24 h.

CONCLUSIONS

A comprehensive study of cooperative stereochemical communication between Fe^{II} centers over nanometer length scales has been conducted using various sizes of self-assembled Fe_4L_6 cages. Stereochemical information from a less bulky chiral amine is transmitted to the Fe^{II}-center inefficiently, although this transfer is amplified by cooperative stereochemical communication between four Fe^{II} centers in the cages. Such communication still takes place even in the larger cages with Fe–Fe distances over 2 nm, independent of ligand axial configuration. In other words, the axial chirality of the ligands in these cages does not appear to affect chiral information transfer between Fe^{II} centers; the transmission of stereochemical information within such cage frameworks occurs independently of the persistence length of the helical conformations of ligand connectors between metal stereocenters.[38–48]

The long-range cooperative[79] stereochemical communication originates from three-dimensional geometric effects within the tetrahedral framework as a whole, namely the energetic preference of the cages to adopt approximate *T*-symmetry because of the distortion of cages incorporating metal centers of opposite handedness. This phenomenon is relevant to polyhedra at all length scales, depending only upon the linkers' degree of offset. This is the first example of long-range stereochemical communication in large three-dimensional architectures that are not helical in nature. These findings may provide a means for the rational design of very large chiral supramolecular architectures for the discrimination and transformation of large chiral guests.

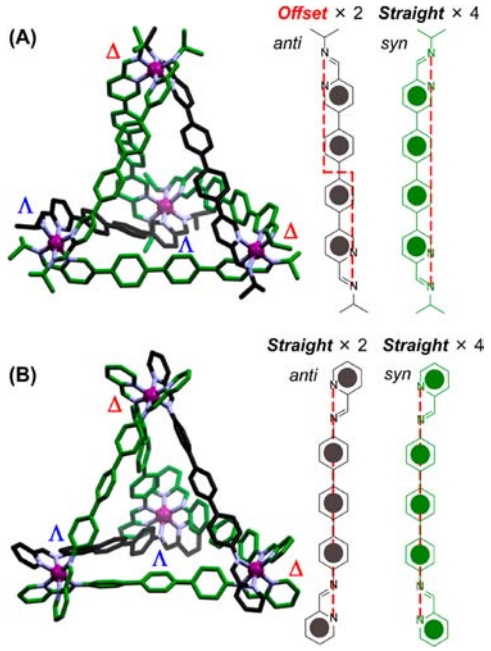

Figure 9. Molecular models of (A) S_4-symmetric $\Delta\Delta\Lambda\Lambda$-$S_4$-**6** and (B) $\Delta\Delta\Lambda\Lambda$-$S_4$-**7** optimized by molecular mechanics (MM+ force field). Black and green ligands denote *anti*- and *syn*-conformations. Hydrogen atoms are omitted for clarity.

EXPERIMENTAL METHODS

General. All reagents and solvents were purchased from commercial sources and used as supplied unless otherwise noted. NMR spectra were recorded on a Bruker Avance DPX400 or DRX500 spectrometer. Chemical shifts are reported in parts per million (δ) from the CHD_2CN residual solvent signal of CD_3CN or the $CHCl_3$ residual solvent signal of $CDCl_3$. ESI-MS was obtained on a Micromass Quattro LC, infused from a Harvard syringe pump at a rate of 10 μL per minute. CD analyses were performed on an Applied Photophysics Chirascan circular dichroism spectrometer. Molecular modeling studies were performed with the use of HyperChem software.

Cage **1a**: Into a 10 mL vial containing CH_3CN (3 mL) were added 6,6′-diformyl-3,3′-bipyridine (30.0 mg, 0.141 mmol) and iron(II) triflate $[Fe(OTf)_2]$ (33.5 mg, 0.095 mmol). The vial was sealed with rubber septum and subjected to three evacuation/nitrogen fill cycles. To this mixture was then added (*S*)-(+)-2-aminobutane (32 μL, 0.31 mmol) via syringe. The solution was stirred overnight at 60 °C. Cage **1a** was precipitated as a purple powder (65.1 mg, 82.4%) by the addition of $^iPr_2O$ and hexane. ^1H NMR (500 MHz, CD_3CN): δ = 9.2 (s, 12H, imine), 8.40 (d, J = 8.0 Hz, 12H, 5,5′-bipyridine), 7.85 (dd, J = 1.8, 8.0 Hz, 12H, 4,4′-bipyridine), 6.44 (s, 12H, 2,2′-bipyridine), 3.69 (m, 12H, $C^{\alpha}H$ 2-aminobutane), 1.55 (d, J = 6.6 Hz, 36H, CH_3 2-aminobutane), 1.00 (m, 24H, CH_2 2-aminobutane), 0.53 (m, 36H, CH_2CH_3 2-aminobutane). ^{13}C NMR(CD_3CN, 125 MHz): δ = 171.9, 159.5, 154.1, 140.0, 136.7, 129.7, 67.2, 30.4, 21.1, 10.1. ESI-MS (positive) m/z: $[M–2CF_3SO_3]^{2+}$: 1526.02, $[M–3CF_3SO_3]^{3+}$: 967.84, $[M–4CF_3SO_3]^{4+}$: 688.59, $[M–5CF_3SO_3]^{5+}$: 521.07, $[M–6CF_3SO_3]^{6+}$: 409.27.

dx.doi.org/10.1021/ja306615d | J. Am. Chem. Soc. 2012, 134, 15528–15537

Cage **1b**: Into a 10 mL vial containing CH_3CN (2 mL) were added 6,6′-diformyl-3,3′-bipyridine (10.0 mg, 0.047 mmol), (*R*)-(−)-phenylglycinol (13.6 mg, 0.099 mmol), and $Fe(OTf)_2$ (11.2 mg, 0.032 mmol). The vial was sealed with rubber septum and subjected to three evacuation/nitrogen fill cycles. The solution was stirred overnight at 60 °C. Cage **1b** was precipitated as a purple powder (27.9 mg, 86.4%) by the addition of $^iPr_2O$. ^1H NMR (500 MHz, CD_3CN): δ = (for **1b** encapsulating OTf^-) 9.33 (s, 12H, imine), 7.64 (d, J = 8.1 Hz, 12H, 5,5′-bipyridine), 7.35−7.07 (overlapping, 4,4′-bipyridine, 2,3,4-phenyl), 6.03 (d, J = 1.6 Hz, 12H, 2,2′-bipyridine), 5.80 (dd, J = 3.2, 9.9 Hz, 12H, C$^{\alpha}$*H* phenylglycinol), 4.45−4.31 + 3.85 (overlapping, CH_2 + O*H* phenylglycinol); (for empty cage **1b**) 9.28 (s, 12H, imine), 7.58 (d, J = 8.1 Hz, 12H, 5,5′-bipyridine), 7.28−7.07 (overlapping, 4,4′-bipyridine, 2,3,4-phenyl), 5.97 (d, J = 1.6 Hz, 12H, 2,2′-bipyridine), 5.80 (overlapping, C$^{\alpha}$H phenylglycinol), 4.45−4.31 + 3.85 (overlapping, CH_2 + O*H* phenylglycinol). ^{13}C NMR (CD_3CN, 125 MHz): δ = (for **1b** encapsulating OTf^-) 172.7, 160.17, 150.7, 140.4, 136.9, 136.3, 129.9, 129.4, 129.1, 127.2, 75.5, 65.7; (for empty cage **1b**) 172.5, 159.1, 153.6, 139.3, 136.4, 136.2, 129.6, 129.0, 128.9, 75.4, 65.9. ESI-MS (positive) m/z: $[M-3CF_3SO_3]^{3+}$: 1223.76, $[M-4CF_3SO_3]^{4+}$: 880.59, $[M-5CF_3SO_3]^{5+}$: 674.67.

Cage **2a**: Cage **2a** was prepared in a similar manner to that for **1a**. Yield (42.7 mg, 85.5%). ^1H NMR (500 MHz, CD_3CN): δ = 9.11 (s, 12H, imine), 8.37 (d, J = 7.9 Hz, 12H, 3,3′-bipyridine), 8.04 (d, J = 7.9 Hz, 12H, 4,4′-bipyridine), 7.11 (s, 12H, 6,6′-bipyridine), 6.87 (s, 12H, ArH), 3.46 (m, 12H, C$^{\alpha}$*H* 2-aminobutane), 1.91 (s, 36H, ArCH_3), 1.50 (d, J = 6.3, 36H, CH_3 2-aminobutane), 1.19 + 0.56 (m + m, 24H, CH_2 2-aminobutane), 0.45 (m, 36H, CH_2CH_3 2-aminobutane). ^{13}C NMR (CD_3CN, 125 MHz): δ = 172.2, 159.4, 153.8, 142.5, 140.8, 137.2, 134.2, 132.7, 130.3, 65.0, 30.9, 21.1, 19.9, 10.1. ESI-MS (positive) m/z: $[M-3CF_3SO_3]^{3+}$: 117.92, $[M-4CF_3SO_3]^{4+}$: 844.74, $[M-5CF_3SO_3]^{5+}$: 645.98, $[M-6CF_3SO_3]^{6+}$: 513.50, $[M-7CF_3SO_3]^{7+}$: 418.80.

Cage and helicate **2b**: These were prepared in a similar manner to that for **1b**. Yield (42.7 mg, 85.5%). ^1H NMR (500 MHz, CD_3CN): δ = (for cage **2b**) 9.20 (s, 12H, imine), 7.61 (overlapping, 3,3′-, 4,4′-bpyridine), 7.20−7.01 (overlapping, 2,3,4-phenyl phenylglycinol), 6.64 (s, 12H, 6,6′-bipyridine), 6.62 (s, 12H, ArH), 5.80 (dd, J = 8.8, 3.2 Hz, C$^{\alpha}$H phenylglycinol), 4.48−3.91 (overlapping, CH_2 + O*H* phenylglycinol), 1.77 (s, 36H, ArCH_3); (for helicate 2b) 8.88 (s, 6H, imine), 7.93 (dd, 6H, J = 8.0, 1.5 Hz, 3,3′-bipyridine), 7.49 (d, 6H, J = 8.0 Hz, 4,4′-bipyridine), 7.20−7.01 (overlapping, 2,3,4-phenyl, phenylglycinol), 6.89 (s, 6H, ArH), 6.84 (d, J = 7.5 Hz, phenyl phenlglycinol), 6.48 (s, 6H, 6,6′-bipyridine), 5.93 (dd, 6H, J = 10.0, 3.3 Hz, C$^{\alpha}$H phenylglycinol), 4.48−3.91 (overlapping, CH_2 + O*H* phenylglycinol), 1.51 (s, 18H, ArCH_3). ^{13}C NMR (CD_3CN, 125 MHz): δ = (for cage **2b**) 172.7, 158.9, 152.8, 140.8, 139.9, 136.9, 136.7, 134.2, 132.7, 130.0, 129.9, 1291, 127.2, 74.5, 65.9, 20.5; (for helicate **2b**) 171.8, 158.3, 152.2, 139.8, 137.9, 13.9, 136.1, 135.9, 134.4, 130.5, 129.7, 129.2, 127.1, 75.1, 65.2, 19.3. ESI-MS (positive) m/z: [M(helicate)−$2CF_3SO_3]^{2+}$: 1036.95, [M(helicate)−$3CF_3SO_3]^{3+}$: 641.33, [M-(helicate)−$4CF_3SO_3]^{4+}$: 443.80, [M(cage)−$5CF_3SO_3]^{5+}$: 799.59.

Cage **2′a**: Cage **2′a** was prepared in a similar manner to that for **1a**. Yield (30.7 mg, 69.8%). ^1H NMR (500 MHz, CD_3CN): δ = 9.06 (s, 12H, imine), 8.58 (d, 12H, J = 7.9 Hz, 3,3′-bpyridine), 8.43 (d, 12H, J = 8.1 Hz, 4,4′-bpyridine), 7.34 (s, 24H, ArH), 6.90 (s, 12H, 6,6′-bpyridine), 3.73 (bs, 12H, C$^{\alpha}$H 2-aminobutane), 1.58 (d, 36H, J = 6.3 Hz, CH_3 2-aminobutane), 1.04 + 0.70 (m + m, 24H, CH_2 2-aminobutane), 0.52 (t, 36H, J = 7.1 Hz, CH_2CH_3 2-aminobutane). ^{13}C NMR (CD_3CN, 125 MHz): δ = 171.2, 159.0, 152.3, 138.7, 137.3, 135.7, 130.1, 128.3, 66.5, 30.8, 21.1, 10.0. ESI-MS (positive) m/z: $[M-3CF_3SO_3]^{3+}$: 1119.81, $[M-4CF_3SO_3]^{4+}$: 802.64, $[M-5CF_3SO_3]^{5+}$: 612.31, $[M-6CF_3SO_3]^{6+}$: 485.28, $[M-7CF_3SO_3]^{7+}$: 394.68.

Cage **2′b**: Cage **2′b** was prepared in a similar manner to that for **1b**. Yield (40.9 mg, 77.3%). ^1H NMR (500 MHz, CD_3CN): δ = 9.06 (s, 12H, imine), 7.98 (dd, 12H, J = 8.3, 1.7 Hz, 3,3′-bipyridine), 7.56 (d, 12H, J = 8.2 Hz, 4,4′-bipyridine), 7.14 (s, 24H, ArH), 7.04 (t, 12H, J = 7.0 Hz, 4-phenyl phenylglycinol), 6.95−6.89 (overlapping, 2,3-phenyl), 6.80 (d, 12H, J = 1.2 Hz, 6,6′-bipyridine), 5.77 (m, 12H, C$^{\alpha}$*H* phenylglycinol), 4.29−4.22 + 3.95 (overlapping + m, O*H* + CH_2 phenylglycinol). ^{13}C NMR (CD_3CN, 125 MHz): δ = 172.0, 158.5, 151.2, 138., 136.9, 136.3, 135.8, 129.8, 129.6, 128.9, 128.1, 127.0, 75.0, 65.7. ESI-MS (positive) m/z: $[M-3CF_3SO_3]^{3+}$: 1376.12, $[M-4CF_3SO_3]^{4+}$: 994.67, $[M-5CF_3SO_3]^{5+}$: 765.97, $[M-6CF_3SO_3]^{6+}$: 613.49.

Cage **3a**: Cage **3a** was prepared in a similar manner to that for **1a**. Yield (40.9 mg, 74.9%). ^1H NMR (500 MHz, CD_3CN): δ = 9.16 (s, 12H, imine), 8.40 (d, 12H, J = 7.8, 3,3′-bipyridine), 8.18 (bs, 12H, 4,4′-bipyridine), 6.91−6.83 (overlapping, 36H, ArH + 6,6′-bipyridine), 3.71 (bs, 12H, C$^{\alpha}$*H* 2-aminobutane), 1.88−1.82 (m, 72H, ArCH_3), 1.60 (d, 36H, J = 5.8 Hz, CH_3 2-aminobutane), 1.15 + 0.74 (bs + bs, 24H, CH_2 2-aminobutane), 0.55 (bs, 36H, CH_2CH_3 2-aminobutane). ^{13}C NMR (CD_3CN, 125 MHz): δ = 171.4, 158.5, 158.4, 158.3, 155.5, 142.5, 142.4, 142.1, 142.0, 140.1, 135.3, 134.9, 134.8, 133.5, 133.4, 132.5, 132.3, 132.0, 131.8, 131.7, 129.6, 66.0, 30.9, 21.1,19.9, 19.8, 19.7, 19.1, 19.0, 17.9, 10.0, 9.9. ESI-MS (positive) m/z: $[M-4CF_3SO_3]^{4+}$: 1001.01, $[M-5CF_3SO_3]^{5+}$: 771.01, $[M-6CF_3SO_3]^{6+}$: 617.63, $[M-7CF_3SO_3]^{7+}$: 507.98, $[M-8CF_3SO_3]^{8+}$: 425.95.

Cage **3b**: Cage **3b** was prepared in a similar manner to that for **1b**. Yield (54.0 mg, 84.4%). ^1H NMR (500 MHz, CD_3CN): δ = 9.14 (m, 12H, imine), 7.67 (m, 12H, 3,3′-bipyridine), 7.56 (m, 12H, 4,4′-bipyridine), 7.10 (m, 12H, 4-phenyl phenylglycinol), 7.06 (m, 48H, 2,3-phenyl phenylglycinol), 6.82−6.60 (overlapping, 36H, ArH + 6,6′-bipyridine), 5.87 (bs, 12H, C$^{\alpha}$H phenylglycinol), 4.37 + 4.00 (overlapping + m, 36H, O*H* + CH_2 phenylglycinol), 1.86−1.67 (m, 72H, ArCH_3). ^{13}C NMR (CD_3CN, 125 MHz): δ = 172.2, 158.0, 157.9, 154.2, 154.1, 142.2, 142.1, 141.0, 139.6, 139.5, 139.4, 136.5, 135.4, 135.3, 135.0, 134.9, 134.8, 133.1, 132.3, 131.7, 129.8, 129.0, 127.2, 127.1, 74.9, 65.7, 19.7, 19.6, 19.2, 18.9. ESI-MS (positive) m/z: $[M-4CF_3SO_3]^{4+}$: 1193.04, $[M-5CF_3SO_3]^{5+}$: 924.68, $[M-6CF_3SO_3]^{6+}$: 745.71, $[M-7CF_3SO_3]^{7+}$: 617.88.

Cage **4a**: Cage **4a** was prepared in a similar manner to that for **1a**. Yield (36.9 mg, 74.0%). ^1H NMR (500 MHz, CD_3CN): δ = 9.15 (s, 12H, imine), 8.40 (d, 12H, J = 6.9 Hz, 3,3′-bipyridine), 8.21 (bs, 12H, 4,4′-bipyridine), 6.98−6.89 (overlapping, 48H, ArH + 6,6′-bipyridine), 3.71 (bs, 12H, C$^{\alpha}$H 2-aminobutane), 1.98 (overlapping, ArCH_3), 1.61 (s, 36H, CH_3 2-aminobutane), 1.18 + 0.78 (bs + bs, 24H, CH_2 2-aminobutane), 0.54 (bs, 36H, CH_2CH_3 2-aminobutane). ^{13}C NMR (CD_3CN, 125 MHz): δ = 171.7, 158.7, 154.7, 143.4, 143.3, 142.7, 140.6, 140.5, 135.1, 133.8, 133.7, 133.6, 133.5, 133.3, 132.9, 131.8, 131.6, 131.4, 131.3, 131.2, 129.9, 65.8, 30.9, 21.1, 20.0, 19.4, 19.3, 19.2, 9.91. ESI-MS (positive) m/z: $[M-4CF_3SO_3]^{4+}$: 1157.15, $[M-5CF_3SO_3]^{5+}$: 895.97, $[M-6CF_3SO_3]^{6+}$: 721.77, $[M-7CF_3SO_3]^{7+}$: 597.29, $[M-8CF_3SO_3]^{8+}$: 504.08.

Cage **4b**: Cage **4b** was prepared in a similar manner to that for **1b**. Yield (37.5 mg, 65.6%). ^1H NMR (500 MHz, CD_3CN): δ = 9.12 (m, 12H, imine), 7.74 (bs, 12H, 3,3′-bipyridine), 7.56 (bs, 12H, 4,4′-bipyridine), 7.17 (bs, 12H, 4-phenyl phenylglycinol), 7.11−7.04 (m, 48H, 2,3-phenyl phenylglycinol), 6.90−6.74 (overlapping, 48H, ArH + 6,6′-bipyridine), 5.87 (bs, 12H, C$^{\alpha}$*H* phenylglycinol), 4.36 + 4.00 (overlapping + m, 36H, O*H* + CH_2 phenylglycinol), 1.90 (overlapping, ArCH_3). ^{13}C NMR (CD_3CN, 125 MHz): δ = 172.2, 158.3, 153.4, 143.2, 143.1, 141.4, 140.6, 140.5, 140.4, 139.6, 136.6, 136.5, 135.1, 135.0, 134.9, 133.7, 133.6, 133.5, 133.0, 131.6, 131.4, 131.3, 131.1, 129.8, 129.4, 129.1, 127.1, 74.9, 65.7, 20.4, 19.4, 19.3, 19.2, 19.1. ESI-MS (positive) m/z: $[M-4CF_3SO_3]^{4+}$: 1349.08, $[M-5CF_3SO_3]^{5+}$: 1049.67, $[M-6CF_3SO_3]^{6+}$: 849.84, $[M-7CF_3SO_3]^{7+}$: 707.07, $[M-8CF_3SO_3]^{8+}$: 600.08.

■ ASSOCIATED CONTENT

Ⓢ Supporting Information

Synthetic procedures and characterizations of ligands **2**-**4** and mononuclear complex **5**, and spectroscopic data. This material is available free of charge via the Internet at http://pubs.acs.org.

AUTHOR INFORMATION

Corresponding Author

jrn34@cam.ac.uk; stoddart@northwestern.edu

Notes

The authors declare no competing financial interest.

ACKNOWLEDGMENTS

This work was supported by the European Research Council and the Non-Equilibrium Energy Research Center, which is an Energy Frontier Research Center funded by the U.S. Department of Energy, Offices of Basic Energy Sciences under award number DE-SC0000989. N.O. thanks the Japan Society for Promotion of Science (JSPS) postdoctoral fellowship for young scientists (no. 2692). S.G. thanks the Swiss National Science Foundation for financial support. J.F.S. acknowledges support from the World Class University (WCU) Program (R31-2008-000-10055) at KAIST in Korea.

REFERENCES

(1) Ward, M. D. *Chem. Commun.* **2009**, 4487−4499.
(2) Jin, P.; Dalgarno, S. J.; Atwood, J. L. *Coord. Chem. Rev.* **2010**, *254*, 1760−1768.
(3) Saalfrank, R. W.; Maid, H.; Scheurer, A. *Angew. Chem., Int. Ed.* **2008**, *47*, 8794−8824.
(4) Chakrabarty, R.; Mukherjee, P. S.; Stang, P. J. *Chem. Rev.* **2011**, *111*, 6810−6918.
(5) Fujita, M.; Tominaga, M.; Hori, A.; Therrien, B. *Acc. Chem. Res.* **2005**, *38*, 369−378.
(6) Tranchemontagne, D. J.; Ni, Z.; O'Keeffe, M.; Yaghi, O. M. *Angew. Chem., Int. Ed.* **2008**, *47*, 5136−5147.
(7) Sumida, K.; Rogow, D. L.; Mason, J. A.; McDonald, T. M.; Bloch, E. D.; Herm, Z. R.; Bae, T.-H.; Long, J. R. *Chem. Rev.* **2012**, *112*, 724−781.
(8) Zhang, X. X.; Bradshaw, J. S.; Izatt, R. M. *Chem. Rev.* **1997**, *97*, 3313−3362.
(9) Rivera, J. M.; Martin, T.; Rebek, J. *Science* **1998**, *279*, 1021−1023.
(10) Ishi-i, T.; Mateos-Timoneda, M. A.; Timmerman, P.; Crego-Calama, M.; Reinhoudt, D. N.; Shinkai, S. *Angew. Chem., Int. Ed.* **2003**, *42*, 2300−2305.
(11) Fiedler, D.; Leung, D. H.; Bergman, R. G.; Raymond, K. N. *J. Am. Chem. Soc.* **2004**, *126*, 3674−3675.
(12) Liu, T.; Liu, Y.; Xuan, W.; Cui, Y. *Angew. Chem., Int. Ed.* **2010**, *49*, 4121−4124.
(13) Xuan, W.; Zhang, M.; Liu, Y.; Chen, Z.; Cui, Y. *J. Am. Chem. Soc.* **2012**, *134*, 6904−6907.
(14) Fiedler, D.; Leung, D. H.; Bergman, R. G.; Raymond, K. N. *Acc. Chem. Res.* **2005**, *38*, 349−358.
(15) Nakamura, A.; Inoue, Y. *J. Am. Chem. Soc.* **2005**, *127*, 5338−5339.
(16) Nishioka, Y.; Yamaguchi, T.; Kawano, M.; Fujita, M. *J. Am. Chem. Soc.* **2008**, *130*, 8160−8161.
(17) Yoshizawa, M.; Klosterman, J. K.; Fujita, M. *Angew. Chem., Int. Ed.* **2009**, *48*, 3418−3438.
(18) Murase, T.; Peschard, S.; Horiuchi, S.; Nishioka, Y.; Fujita, M. *Supramol. Chem.* **2011**, *23*, 199−208.
(19) Mal, P.; Schultz, D.; Beyeh, K.; Rissanen, K.; Nitschke, J. R. *Angew. Chem., Int. Ed.* **2008**, *47*, 8297−8301.
(20) Mal, P.; Breiner, B.; Rissanen, K.; Nitschke, J. R. *Science* **2009**, *324*, 1697−1699.
(21) Hristova, Y. R.; Smulders, M. M. J.; Clegg, J. K.; Breiner, B.; Nitschke, J. R. *Chem. Sci* **2011**, *2*, 638−641.
(22) Ousaka, N.; Clegg, J. K.; Nitschke, J. R. *Angew. Chem., Int. Ed.* **2012**, *51*, 1464−1468.
(23) Rowan, S. J.; Cantrill, S. J.; Cousins, G. R. L.; Sanders, J. K. M.; Stoddart, J. F. *Angew. Chem., Int. Ed.* **2002**, *41*, 898−952.
(24) Nitschke, J. R. *Acc. Chem. Res.* **2007**, *40*, 103−112.
(25) Belowich, M. E.; Stoddart, J. F. *Chem. Soc. Rev.* **2012**, *41*, 2003−2024.
(26) Caulder, D. L.; Powers, R. E.; Parac, T. N.; Raymond, K. N. *Angew. Chem., Int. Ed.* **1998**, *37*, 1840−1843.
(27) Stang, P. J.; Olenyuk, B.; Muddiman, D. C.; Smith, R. D. *Organometallics* **1997**, *16*, 3094−3096.
(28) Tidmarsh, I. S.; Taylor, B. F.; Hardie, M. J.; Russo, L.; Clegg, W.; Ward, M. D. *New J. Chem.* **2009**, *33*, 366−375.
(29) Arrgent, S. P.; Riis-Johannessen, T.; Jeffery, J. C.; Harding, L. P.; Ward, M. D. *Chem. Commun.* **2005**, 4647−4649.
(30) Albrecht, M.; Burk, S.; Weis, P. *Synthesis* **2008**, 2963−2967.
(31) Salfrank, R. W.; Demleitner, B.; Glaser, H.; Maid, H.; Bathelt, D.; Hampel, F.; Bauer, W.; Teichert, M. *Chem.—Eur. J.* **2002**, *8*, 2679−2683.
(32) Cotton, F. A.; Murillo, C. A.; Yu, R. *Dalton Trans.* **2005**, 3161−3165.
(33) Meng, W.; Clegg, J. K.; Thoburn, J. D.; Nitschke, J. R. *J. Am. Chem. Soc.* **2011**, *133*, 13652−13660.
(34) Beissel, T.; Powers, R. E.; Raymond, K. N. *Angew. Chem., Int. Ed. Engl.* **1996**, *35*, 1084−1086.
(35) Beissel, T.; Powers, R. E.; Parac, T. N.; Raymond, K. N. *J. Am. Chem. Soc.* **1999**, *121*, 4200−4206.
(36) Saalfrank, R. W.; Maid, H.; Scheurer, A.; Puchta, R.; Bauer, W. *Eur. J. Inorg. Chem.* **2010**, 2903−2906.
(37) Paul, R. L.; Argent, S. P.; Jeffery, J. C.; Harding, L. P.; Lynam, J. M.; Ward, M. D. *Dalton Trans.* **2004**, 3453−3458.
(38) Green, M. M.; Reidy, M. P.; Johnson, R. J.; Darling, G.; Oleary, D. J.; Willson, G. *J. Am. Chem. Soc.* **1989**, *111*, 6452−6454.
(39) Green, M. M.; Garetz, B. A.; Munoz, B.; Chang, H.; Hoke, S.; Cooks, R. G. *J. Am. Chem. Soc.* **1995**, *117*, 4181−4182.
(40) Green, M. M.; Peterson, N. C.; Sato, T.; Teramoto, A.; Cook, R.; Lifson, S. *Science* **1995**, *268*, 1860−1866.
(41) Green, M. M.; Park, J.-W.; Sato, T.; Teramoto, A.; Lifson, S.; Selinger, R. L. B.; Selinger, J. V. *Angew. Chem., Int. Ed.* **1999**, *38*, 3138−3154.
(42) Cornelissen, J. J. L. M.; Rowan, A. E.; Nolte, R. J. M.; Sommerdijk, N. A. J. M. *Chem. Rev.* **2001**, *101*, 4039−4070.
(43) Fujiki, M. *Macromol. Rapid Commun.* **2001**, *22*, 539−563.
(44) Yashima, E.; Maeda, K.; Iida, H.; Furusho, Y.; Nagai, K. *Chem. Rev.* **2009**, *109*, 6102−6211.
(45) Mateos-Timoneda, M. A.; Crego-Calama, M.; Reinhoudt, D. N. *Supramol. Chem.* **2005**, *17*, 67−79.
(46) Palmans, A. R. A.; Meijer, E. W. *Angew. Chem., Int. Ed.* **2007**, *46*, 8948−8968.
(47) Pijper, D.; Feringa, B. L. *Soft Matter* **2008**, *4*, 1349−1372.
(48) De Greef, T. F. A.; Smulders, M. M. J.; Wolffs, M.; Schenning, A. P. H. J.; Sijbesma, R. P.; Meijer, E. W. *Chem. Rev.* **2009**, *109*, 5687−5754.
(49) Clayden, J.; Lund, A.; Vallverdú, L; Helliwell, M. *Nature* **2004**, *431*, 966−971.
(50) Clayden, J.; Castellanos, A.; Solà, J.; Morris, G. A. *Angew. Chem., Int. Ed.* **2009**, *48*, 5962−5965.
(51) Clayden, J. *Chem. Soc. Rev.* **2009**, *38*, 817−829.
(52) Ousaka, N.; Inai, Y. *J. Org. Chem.* **2009**, *74*, 1429−1439.
(53) Ousaka, N.; Takayama, Y.; Iida, H.; Yashima, E. *Nat. Chem.* **2011**, *3*, 856−861.
(54) Maeda, K.; Matsuda, M.; Nakano, T.; Okamoto, Y. *Polym. J.* **1995**, *27*, 141−146.
(55) Clayden, J.; Lemiègre, L.; Morris, G. A.; Pickworth, M.; Snape, T. J.; Jones, L. H. *J. Am. Chem. Soc.* **2008**, *130*, 15193−15202.
(56) Boddaert, T.; Solà, J.; Helliwell, M.; Clayden, J. *Chem. Commun.* **2012**, *48*, 3397−3399.
(57) Lörtscher, E.; Elbing, M.; Tschudy, M.; Hänisch, C. v.; Weber, H. B.; Mayor, M.; Riel, H. *ChemPhysChem* **2008**, *9*, 2252−2258.
(58) Wenger, O. S. *Chem. Soc. Rev.* **2011**, *40*, 3538−3550.
(59) Pasco, S. T.; Baker, G. L. *Synth. Met.* **1997**, *84*, 275−276.
(60) Grunder, S.; Stoddart, J. F. *Chem. Commun.* **2012**, *48*, 3158−3160.

(61) Howson, S. E.; Allan, L. E. N.; Chmel, N. P.; Clarkson, G. J.; van Gorkum, R.; Scott, P. *Chem. Commun.* **2009**, 1727−1729.
(62) Howson, S. E.; Allan, L. E. N.; Chmel, N. P.; Clarkson, G. J.; Deeth, R. J.; Faulkner, A. D.; Simpson, D. H.; Scott, P. *Dalton. Trans.* **2011**, *40*, 10416−10433.
(63) Howson, S. E.; Bolhuis, A.; Brabec, V.; Clarkson, G. J.; Malina, J.; Rodger, A.; Scott, P. *Nat. Chem.* **2012**, *4*, 31−36.
(64) Dragna, J. M; Pescitelli, G.; Tran, L.; Lynch, V. M.; Anslyn, E. V.; Di Bari, L. *J. Am. Chem. Soc.* **2012**, *134*, 4398−4407.
(65) Miyaura, N.; Yamada, K.; Suzuki, A. *Tetrahedron Lett.* **1979**, *36*, 3437−3440.
(66) Miyaura, N.; Suzuki, A. *Chem. Rev.* **1995**, *95*, 2457−2483.
(67) *HyperChem*, version 8.0.3.; Hypercube, Inc.: Gainsville, FL, 2007.
(68) *WINNMR*, version 950901.0; Bruker Instruments, Inc. : Billerica, MA, 1995.
(69) Ziegler, M.; von Zelewsky, A. *Coord. Chem. Rev.* **1998**, *177*, 257−300.
(70) Telfer, S. G.; Tajima, N.; Kuroda, R. *J. Am. Chem. Soc.* **2004**, *126*, 1408−1418.
(71) Bloomfield, V. A.; Crothers, D. M.; Tinoco, I. *Physical Chemistry of Nucleic Acids*; Harper & Row: New York, 1974.
(72) Cantor, C. R.; Schimmel, P. R. *Biophysical Chemistry*; Freeman, New York, 1980.
(73) Nelson, J. C.; Saven, J. G.; Moore, J.; S. Wolynes, P. G. *Science* **1997**, *277*, 1793−1796.
(74) Knof, U.; Von Zelewsky, A. *Angew. Chem., Int. Ed.* **1999**, *38*, 303−322.
(75) Bilbeisi, R. A.; Clegg, J. K.; Elgrishi, N.; de Hatten, X.; Devillard, M.; Breiner, B.; Mal, P.; Nitschke, J. R. *J. Am. Chem. Soc.* **2012**, *134*, 5110−5119.
(76) Scherer, M.; Caulder, D. L.; Johnson, D. W.; Raymond, K. N. *Angew. Chem., Int. Ed.* **1999**, *38*, 1588−1592.
(77) Glasson, C. R. K.; Meehan, G. V.; Clegg, J. K.; Lindoy, L. F.; Smith, J. A.; Keene, F. R.; Motti, C. *Chem.—Eur. J.* **2008**, *14*, 10535−10538.
(78) Glasson, C. R. K.; Meehan, G. V.; Motti, C. A.; Clegg, J. K.; Turner, P.; Jensen, P.; Lindoy, L. F. *Dalton Trans.* **2011**, *40*, 10481−10490.
(79) As discussed in refs 38−48, the terms "cooperative" and "cooperativity" used in this paper refer to stereochemical communication between stereocenters, as distinct from, yet conceptually related to, the idea of "cooperativity" in self-assembling processes: Ercolani, G. *J. Am. Chem. Soc.* **2003**, *125*, 16097−16103.